The stratospheric pathway for Arctic impacts on mid-latitude climate

Tetsu Nakamura[1,2]*, Koji Yamazaki[1,2], Katsushi Iwamoto[3], Meiji Honda[4], Yasunobu Miyoshi[5], Yasunobu Ogawa[6,7], Yoshihiro Tomikawa[6,7], and Jinro Ukita[4]

[1] Arctic Environmental Research Center, National Institute of Polar Research, Tokyo 190-8518, Japan

[2] Faculty of Environmental Earth Science, Hokkaido University, Hokkaido 060-0810, Japan

[3] Mombetsu city government, Hokkaido 094-8707, Japan

[4] Department of Environmental Science, Niigata University, Niigata 950-2181, Japan

[5] Department of Earth and Planetary Sciences, Kyushu University, Fukuoka 812-8581, Japan

[6] Space and Upper Atmospheric Sciences Group, National Institute of Polar Research, Tokyo 190-8518, Japan

[7] SOKENDAI (The Graduate University for Advanced Studies), Tokyo 190-8518, Japan

*Corresponding author: T. Nakamura (nakamura.tetsu@ees.hokudai.ac.jp)

A revised version submitted to Geophysical Research Letters, 17 February 2016

Key points

- Stratospheric dynamics is crucial for Arctic sea-ice and mid-latitude climate linkage
- Reduced stratospheric wave mean-flow interaction much alters the sea ice impacts on the surface
- Representation of the whole stratosphere is indispensable for realistic climate predictions

Abstract

Recent evidence from both observations and model simulations suggests that an Arctic sea-ice reduction tends to cause a negative Arctic Oscillation (AO) phase with severe winter weather in the Northern Hemisphere, which is often preceded by weakening of the stratospheric polar vortex. Although this evidence hints at a stratospheric involvement in the Arctic–mid-latitude climate linkage, the exact role of the stratosphere remains elusive. Here we show that tropospheric AO response to the Arctic sea-ice reduction largely disappears when suppressing the stratospheric wave–mean flow interactions in numerical experiments. The results confirm a crucial role of the stratosphere in the sea-ice impacts on the mid-latitudes by coupling between the stratospheric polar vortex and planetary-scale waves. Those results and consistency with observation-based evidence suggest that a recent Arctic sea-ice loss is linked to mid-latitudes extreme weather events associated with the negative AO phase.

Index Terms

0750 Sea ice
1605 Abrupt/rapid climate change
1620 Climate dynamics
3349 Polar meteorology
3362 Stratosphere/troposphere interactions

Keywords

Arctic sea-ice reduction, Arctic Oscillation, Severe weather, Polar amplification, Polar vortex weakening, Wave-mean flow interaction

1. Introduction

In the global climate system the atmosphere has an important role in connecting climates of different regions, a phenomenon called atmospheric teleconnection, in response to a range of surface boundary conditions. Thus, in investigations of intraseasonal to seasonal climate links between the Arctic and the mid-latitudes, it is essential to ask if and how an observed Arctic sea-ice loss, by affecting atmospheric circulation aloft, is able to influence weather and climate in remote regions [*Deser et al.,* 2010]. Both observations and numerical simulations have shown that a reduction in the Arctic summer-to-fall sea-ice extent, particularly over the Barents-Kara Sea, modulates atmospheric circulation in the subsequent fall-to-winter so as to strengthen the Siberia High, which often brings severe winters to eastern Eurasia [*Honda et al.,* 2009; *Overland et al.,* 2011; *Hospsch et al.,* 2012; *Orsolini et al.,* 2012; *Mori et al.,* 2014]. In addition, when the sea-ice cover is low, Northern Hemisphere jets tend to meander, and this meandering often brings anomalously cold weather to the mid-latitudes, especially in the Euro-Atlantic sector although there is a debate on this notion especially in terms of the choice of a metric [*Francis and Vavrus,* 2012; *Barnes,* 2013; *Screen and Simmonds,* 2014]. Anomalously cold winters and meandering jets occur more frequently during the negative phase of the Arctic Oscillation (AO) [*Thompson and Wallace,* 2001; *Barriopedro and Garcia-Herrera,* 2006; and *Vavrus et al.,* 2006], which is the predominant variability pattern of the Northern Hemisphere winter climate [*Thompson and Wallace,* 1998]. Dynamically, the negative AO phase represents the atmospheric state in which a larger air mass resides over the polar region and is associated with weak westerlies, anomalously meandering jets in the upper troposphere, and anomalous surface weather patterns.

Recent observational studies have reported that, following a summer with a low Arctic sea-ice cover, upward propagation of planetary-scale waves is enhanced in late fall and early winter, which leads to a weakened stratospheric polar vortex and subsequent surface signals [*Jaiser et al.,* 2012; *King et al.,* 2015]. On the other hand, modelling studies have also provided supporting evidence for this dynamical process in the stratosphere and troposphere as responses to changes in both sea-ice [*Orsolini et al.,* 2012; *Kim et al.,* 2014; *Nakamura et al.,* 2015] and snow boundary conditions [*Fletcher et al.,* 2007; *Peings et al.,* 2012]. Other modelling studies have contradicting results on the AO phase as an Arctic sea-ice response [*Cai et al.,* 2012].

88 At present the exact role of the stratospheric processes in the Arctic–mid-latitude
89 climate linkage under the present climatic conditions, especially that associated with an
90 observed rapid sea-ice loss, remains unclear. Observationally, it is very difficult to
91 assess the impact of sea ice or snow alone because they might co-vary [*Liu et al.,* 2012;
92 *Wegmann et al.,* 2015]. Although in principle modelling studies can isolate the impacts
93 of sea ice and snow, few studies to date have used a fully stratosphere-resolving (i.e.,
94 high-top) model and explicitly examined the role of the stratosphere in the Arctic–
95 mid-latitude climate linkage [e.g., *Fletcher et al.,* 2009]. A recent study based on a
96 high-top model by *Sun et al.* [2015] found that reduced sea-ice in the Arctic would lead
97 to significant modulation of the AO behaviour and consequential impacts on the surface
98 climate through stratospheric wave-mean flow interactions. However, their focus was
99 on a projected sea-ice response in a centennial time scale, and there has been no
100 modelling study examining impacts of an observed rapid Arctic sea-ice loss with an
101 attention on stratospheric processes using a high-top model. Nor is there a model study
102 directly investigating the role of stratospheric wave-mean flow interactions in the
103 context of the sea-ice impacts on mid-latitudes climate.
104 Here we show that, based on numerical experiments using a high-top atmospheric
105 general circulation model [*Nakamura et al.,* 2015] that has already shown sea-ice
106 impacts on the stratosphere highly consistent with observations, mid-latitude surface
107 signals as a response to the Arctic sea-ice reduction disappear when artificially
108 suppressing stratospheric wave–mean flow interaction. The results confirm the active
109 role of the stratosphere in the Arctic–mid-latitude climate linkage. Then, from *a*
110 *posteriori* analysis we argue that an observed reduction in sea ice alone can sufficiently
111 affect atmospheric circulation to influence surface climate via the stratospheric pathway.
112
113 **2. Methods**
114 **2.1. Data**
115 The Merged Hadley–National Oceanic and Atmospheric Administration/Optimum
116 Interpolation Sea Surface Temperature (SST) and Sea-ice Concentration (SIC) datasets
117 [*Hurrell et al.,* 2008] for the period 1979–2011 were used for the boundary conditions
118 of the model. The model simulated turbulent heat fluxes over ice-covered and
119 open-water grid cells in the Arctic Ocean were comparable to observation-based fluxes.
120 To demonstrate the influence of actual sea-ice reductions during recent decades, we

121 defined *Early* (5-year average of 1979–1983) and *Late* (2005–2009) periods, when the
122 ice cover was heavy and light, respectively. The calculated change in sea ice (*Late*
123 minus *Early*) showed large sea-ice reductions in the East Siberian Sea in summer, the
124 Barents-Kara Sea and Bering Strait in winter, and the Okhotsk Sea in late winter (see
125 Figure 1 of *Nakamura et al.* [2015]).
126
127 **2.2. Model and experimental design**
128 We used the Atmospheric General Circulation Model for the Earth Simulator (AFES)
129 version 4.1 with triangular truncation at horizontal wavenumber 79 (T79; horizontal
130 resolution approximately 1.5°), 56 vertical levels, and the model top at about 60 km. We
131 performed three sensitivity experiments (*FREE*, *RS10*, and *RS30*), each consisting of
132 two perpetual model runs (*HICE* and *LICE*) using sea-ice conditions of the *Early* or
133 *Late* periods as summarized in Table 1.
134 The *FREE* experiment was the same as the sensitivity experiment performed in our
135 previous study [*Nakamura et al.,* 2015], in which sea-ice conditions during the *Early*
136 and *Late* periods were used as the boundary conditions for high sea-ice (*HICE*) and low
137 sea-ice (*LICE*) runs, respectively. Boundary conditions of sea-surface temperature
138 (SST) were identical, and the other external forcings were fixed as follows: 380 ppmv
139 for CO_2, 1.8 ppmv for CH_4, and the monthly climatological mean O_3 for 1979–2011,
140 obtained from the Japanese 25-year Reanalysis/Japan Meteorological Agency Climate
141 Data Assimilation System reanalysis data. Default values of aerosol and incident solar
142 radiation were used. More detailed description of the experimental settings can be found
143 in our previous paper [*Nakamura et al.,* 2015]. Using the 60-year output of the two runs,
144 which followed an 11-year spin-up, we examined the atmospheric responses to
145 differences in the sea-ice conditions.
146 The *RS10* experiment differed from *FREE* in that the zonal mean zonal wind above
147 10 hPa was restored at every time step by relaxation toward the climatology of the daily
148 annual cycle in the *HICE* run of *FREE* with a maximum relaxation timescale of 1 day.
149 Relaxation forcing τ^{-1} was zero ($\tau = \infty$) at and below the lowest level of 10 hPa and
150 increased linearly up to 1.0 d^{-1} (τ = 1 day) at the higher level of 3.16 hPa, and was 1.0
151 d^{-1} above that level. The *RS30* experiment was the same as *RS10* except that the lowest
152 level was 31.6 hPa and the higher level was 10 hPa (Supplementary section S1).
153 Because our experiments restored the zonal mean component of the zonal wind but not

the eddy (departure from the zonal mean) component, interaction of the planetary wave and the mean flow was suppressed by damping feedback from the wave to the mean flow rather than by damping the amplitude of the wave itself. By this suppression of wave–mean flow interaction, *RS10* and *RS30* partially emulated the low-top models, which are often used for climate simulations (e.g., phase 3 of the Coupled Model Intercomparison Project, CMIP3). It should be noted that the restoring force leads small biases in the climatological state (discussed in Supplementary section S2). As an additional check on possible changes in the dominant circulation pattern in the troposphere during our restoring experiments, we examined the first empirical orthogonal function (EOF1) in the Northern Hemisphere troposphere in all experiments and confirmed that the AO pattern was the first dominant mode in all experiments.

2.3. Statistics and techniques

In the individual experiments, we examined the differences in the 60-year averages of *LICE* minus *HICE*, in which only the sea-ice difference was responsible for the atmospheric anomalies. Statistical significance was examined by a two-tailed standard *t*-test for pairs of the 60 samples. Transformed Eulerian Mean (TEM) diagnostics were used to determine the vertical component of the EP flux (Fz), an indicator of the upward propagation of planetary-wave activity. The 5-day running means of zonal mean zonal wind and Fz were used for daily temporal anomalies. The polar cap height (PCH) was defined as geopotential height averaged northward of 65°N at each pressure level. Variations of the daily mean PCH during the 90 days of winter (December, January, and February) were used to diagnose the vertical coupling intensity in the three experiments. Eddy geopotential heights were defined as departures of the geopotential height from its zonal mean. The three-dimensional EP flux [*Plumb,* 1985] was used to diagnose the three-dimensional structure of wave activity in the model.

3. Results

3.1. Different sea-ice impacts due to representation of the stratosphere

We evaluated the simulated responses to sea-ice reduction in the Arctic region by subtracting the *HICE* results from the *LICE* results. Hereafter, we refer to these differences as anomalies. In the *FREE* experiment, the geopotential height anomalies in

the upper troposphere at 300 hPa averaged over December, January, and February (DJF) clearly showed the negative AO phase pattern, which is characterized by positive anomalies over the Arctic and negative anomalies in surrounding regions (Fig. 1b). At 2 m height, large negative (cold) air temperature anomalies were found over eastern Siberia and less significant negative anomalies were seen over the Europe and northeastern North America region (Fig. 1c). These results are highly consistent with observations that, following a low summertime sea-ice cover in the Arctic, the wintertime AO tends to be in its negative phase, which brings severe winter weather to Eurasia and the North Atlantic sector [*Francis and Vavrus,* 2012; *Barnes,* 2013; *Cohen et al.,* 2014; *Screen and Simmonds,* 2014; *Kim et al.,* 2014; *Nakamura et al.,* 2015; *Sun et al.,* 2015]. In the stratosphere the signal of the negative AO phase was marked in the geopotential height anomalies at 50 hPa (Fig. 1a).

When restoration was applied, the stratospheric AO signal was not so different (*RS10*) or was slightly weakened (*RS30*). In contrast, no clear AO signal at 300 hPa (Fig. 1b) nor any significant cold anomalies (Fig. 1c) was seen in eastern Siberia. Instead, a significant cold anomaly was seen over North-western North America only in *RS10*. These results show that by damping stratospheric variations, the tropospheric response to the sea-ice reduction was modified in such a way that the negative AO-like pattern and its associated cold anomalies in the troposphere were much subdued or even absent in the experiments with restored stratospheric circulation. Furthermore, the surface temperature anomalies differ among three experiments except for warm anomalies over ice reduction regions, suggesting large natural fluctuations of the temperature responses that hinder to detect sea ice impacts on the surface [*Mori et al.,* 2014].

3.2. Dynamical processes

Central to stratosphere–troposphere coupling is a dynamical process by which planetary-scale waves propagate upward, followed by weakening of the stratospheric polar vortex and the downward progress of its signal back to the troposphere [*Baldwin and Dunkerton,* 2001; *Nishii et al.,* 2011; *Kidston et al.,* 2015]. These components were all clearly identified as responses to sea-ice reduction in the *FREE* experiment. During December–March, an increase in anomalies in the vertical component of the Eliassen-Palm (EP) flux (F_Z) at 100 hPa averaged over the 50–80°N latitude band (a measure of the upward propagation of planetary-scale wave activity) just prior to a

period of negative anomalies in the zonal mean zonal winds at 60°N in the upper stratosphere was followed 1 to 3 weeks later by downward propagation of the stratospheric signal to the troposphere (Fig. 2a and b). These temporal characteristics were further captured by a lead–lag correlation map of polar cap height (PCH) anomalies (Fig. 2c). From the reference height of 100 hPa, the upper stratosphere PCH anomalies led by up to 2 weeks and the tropospheric PCH anomalies lagged on a much shorter timescale; together they indicate slow downward propagation of the stratospheric signal and faster coupling between the lower stratosphere and the troposphere.

These signatures were much reduced in *RS10*. Although similar negative wind anomalies in the stratosphere appeared after some intensification of upward wave propagation in December and January, their amplitudes were smaller, and the signal was less significant compared with the signatures in *FREE*. Importantly, the signal no longer reached the troposphere (Fig. 2a and b). In *RS30*, there was no significant downward propagation of the stratospheric signal (Fig. 2a). One might think that the stratosphere–troposphere coupling would be weak in the restored experiments. On the contrary, at zero lag stratosphere–troposphere coupling was seen in all three experiments (Fig. 2c). Thus, one of the reasons for the lack of a tropospheric signal in *RS10* is that the signal in the lower stratosphere was too weak; this was caused by the unrealistically weak amplitudes of the anomalies in the upper stratosphere (Supplementary Fig. S1b), which therefore no longer propagated to the lower stratosphere. The fact that the lead–lag structure in the upper stratosphere was degraded in a stepwise manner with restoration (Fig. 2c) provides strong evidence for an active stratospheric dynamic role, and at the same time suggests the importance of the upper stratosphere.

To strengthen our case for the critical role of the stratosphere, we examined the details of upward propagation of planetary-scale waves. We note that anomalous upward propagation of planetary-scale waves occurred mainly over eastern Siberia (Fig. 3b) in all three experiments. The co-location of these anomalies with geopotential height anomalies and their respective climatological locations (Fig. 3a and Supplementary section S3) indicated that the deepening of the climatological trough over eastern Siberia is key to the anomalous upward propagation of planetary-scale waves. This robustness of the spatial distribution of the upward propagation across the experiments is expected because restoring the zonal winds did not suppress the

amplitude of the waves; it only suppressed the interaction of the waves with the mean flow. The upward EP flux anomaly in January was persistently positive in *FREE* (purple lines in Fig. 2b), reflecting more frequent occurrence of upward propagating wave packet with longer duration. This suggests the presence of some two-way interactions in which planetary-wave modulation is affected by the stratosphere–troposphere coupling process itself (discussed in Supplementary section S4). That is, the anomalous upward wave propagation is not only induced by the tropospheric wave source but also intensified by the stratospheric circulation changes, as has been suggested previously [*Harnik,* 2009; *Nishii et al.,* 2011].

3.3. Possible snow cover influences

Finally, we examined the possibility that snow-cover changes induced by sea-ice changes could have triggered stratospheric processes. The correlation between the snow-covered area in Siberia (see Supplementary section S5 for details) and the strength of the tropospheric AO was negative ($r = -0.25$; $p = 0.054$) in the *HICE* run of the *FREE* experiment. This result may be taken as evidence for snow-cover impacts on the surface climate in winter [*Fletcher et al.,* 2007; *Fletcher et al.,* 2009; *Peings et al.,* 2012]. However, we found no appreciable difference in the snow-cover extent between the *HICE* and *LICE* runs in the *FREE* experiment. On the basis of this *a posteriori* analysis we argue that changes in sea-ice conditions alone have a sufficiently large and direct influence on atmospheric circulation and onto surface climate via the stratospheric pathway, without invoking indirect impacts from the induced snow-cover changes.

4. Discussion and concluding remarks

It is a challenging task to fully understand the Arctic-mid-latitudes climate linkage, especially the AO phase as a response to changing Arctic climate. Atmospheric circulation responses to sea-ice anomalies vary among different models and experiments, and both positive and negative AO-like responses to the Arctic sea ice changes have been reported [e.g., *Screen and Simmonds,* 2014; *Barnes and Screen*, 2015; *Sun et al*., 2015]. The responses vary depending on an exact period and a region of sea ice anomalies in question (see the discussion in *Sun et al.* [2015]). In this context, it is worth stating that our simulation was based on sea ice anomalies representing rapid

changes over the last three decades with the strongest influence from the late-fall turbulent heat flux anomalies in the Barents-Kara Seas as discussed in *Nakamura et al.* [2015]. Within this framework, our results suggest that the observed Arctic sea-ice variations, by triggering stratospheric processes, have potential to exert significant weather and climate influences on the Northern Hemisphere mid-latitudes. For better understanding of the Arctic-mid-latitudes climate linkage, a comparison with observations in terms of magnitudes of signals with a careful analysis on combined impacts from different sources and pathways are clearly needed in future. In particular, large part of the differences among the previous results can be traced to a different basic state of the stratosphere and/or a particular phase of the responses relative to climatological stationary-wave structure [*Smith et al.,* 2010; *Nishii et al.,* 2011], which will be covered in our future work.

The present results indicate climate models, which contain the whole stratosphere, are indispensable for realistic climate predictions. The stratosphere now appears to be influenced by various sources. Our results place Arctic sea ice in an already long list of forcings, including tropical sea surface temperature (e.g., El Niño-Southern Oscillation), ozone and greenhouse gases, that can affect the stratospheric polar vortex strength with consequential downward influences on the surface climate [*Brönnimann et al.,* 2004; *Manzini et al.,* 2006; *Ineson and Scaife,* 2009; *Kidston et al.,* 2015]. For better climate predictions, besides a deeper understanding of stratosphere–troposphere coupling mechanisms, there is an urgent need to understand the combined influences of these various sources on the stratosphere.

Acknowledgements

We thank K. Dethloff, D. Handorf, and R. Jaiser for helpful discussions and comments. Merged Hadley–NOAA/OI SST and SIC data were obtained from the Climate Data Guide provided by the National Center for Atmospheric Research (NCAR) and University Corporation for Atmospheric Research (UCAR) (https://climatedataguide.ucar.edu/). The AFES simulations were performed on the Earth Simulator at the Japan Agency for Marine–Earth Science and Technology (JAMSTEC). To access our AFES simulation data, contact the corresponding author (nakamura.tetsu@ees.hokudai.ac.jp). This study was supported by the Green Network of Excellence Program (GRENE Program) Arctic Climate Change Research Project and

318 the Japanese Ministry of Education, Culture, Sports, Science and Technology (MEXT)
319 through a Grant-in-Aid for Scientific Research in Innovative Areas 2205. The authors
320 have no competing interests that might be perceived to influence the results and/or
321 discussion reported in this article.
322
323 **References**
324 Baldwin, M. P., T. J. Dunkerton (2001), Stratospheric harbingers of anomalous weather
325 regimes, *Science, 294,* 581–584.
326 Barriopedro, D., and R. Garcia-Herrera (2006), A climatology of Northern Hemisphere
327 blocking, *J. Clim., 19,* 1042–1063, doi:10.1175/JCLI3678.1.
328 Barnes, E. A. (2013), Revisiting the evidence linking Arctic amplification to extreme
329 weather in midlatitudes, *Geophys. Res. Lett., 40,* 1–6.
330 Barnes, E. A., and J. A. Screen (2015), The impact of Arctic warming on the midlatitude
331 jetstream: Can it? Has it? Will it?, *WIREs Climate Change, 6,* 277–286.
332 Brönnimann, S., J. Luterbacher, J. Staehelin, T. M. Svendby, G. Hansen, and T. Svenøe
333 (2004), Extreme climate of the global troposphere and stratosphere in 1940–42 related
334 to El Niño, *Nature, 431,* 971–974.
335 Cai, D., M. Dameris, H. Garny, and T. Runde (2012), Implications of all season Arctic
336 sea-ice anomalies on the stratosphere, *Atmos. Chem. Phys*., *12,* 11819–11831.
337 Cohen, J., J. A. Screen, J. C. Furtado, M. Barlow, D. Whittleston, D. Coumou, J.
338 Francis, K. Dethloff, D. Entekhabi, J. Overland, and J. Jones (2014), Recent Arctic
339 amplification and extreme mid-latitude weather, *Nature Geoscience, 7,* 627–637.
340 Deser, C., R. Tomas, M. Alexander, and D. Lawrence (2010), The seasonal atmospheric
341 response to projected Arctic sea ice loss in the late 21st century, *J. Climate, 23,* 333–
342 351.
343 Fletcher, C. G., P. J. Kushner, and J. Cohen (2007), Stratospheric control of the
344 extratropical circulation response to surface forcing, *Geophys. Res. Lett., 34,* L21802.
345 Fletcher, C. G., S. C. Hardiman, and P. J. Kushner (2009), The Dynamical Response to
346 Snow Cover Perturbations in a Large Ensemble of Atmospheric GCM Integrations, *J.*
347 *Clim., 22,* 1208–1222.
348 Francis, J. A., and S. J. Vavrus (2012), Evidence linking Arctic amplification to extreme
349 weather in mid-latitudes, *Geophys. Res. Lett., 39,* L06801.
350 Harnik, N. (2009), Observed stratospheric downward reflection and its relation to

upward pulses of wave activity, *J. Geophys. Res., 114,* D08120.

Honda, M., J. Inoue, and S. Yamane (2009), Influence of low Arctic sea-ice minima on anomalously cold Eurasian winters, *Geophys. Res. Lett., 36,* L08707.

Hopsch, S., J. Cohen, and K. Dethloff (2012), Analysis of a link between fall Arctic sea ice concentration and atmospheric patterns in the following winter, *Tellus A, 64,* 18624.

Hurrell, J. W., J. J. Hack, D. Shea, J. M. Caron, and J. A. Rosinski (2008), A new sea surface temperature and sea ice boundary dataset for the Community Atmosphere Model, *J. Clim., 21,* 5145–5153.

Ineson, S., and A. A. Scaife (2009), The role of the stratosphere in the European climate response to El Niño, *Nature Geoscience, 2,* 32–36.

Jaiser, R., K. Dethloff, D. Handorf, A. Rinke, and J. Cohen (2012), Impact of sea ice cover changes on the Northern Hemisphere atmospheric winter circulation, *Tellus A, 64,* 11595.

Kidston, J., A. A. Scaife, C. Hardiman, D. M. Mitchell, N. Butchart, M. P. Baldwin, and L. J. Gray (2015), Stratospheric influence on tropospheric jet streams, storm tracks and surface weather, *Nature Geoscience, 8,* 433–440.

Kim, B. M., S. W. Son, S. K. Min, J. H. Jeong, S. J. Kim, Z. Zhang, T. Shim, and J. H. Yoon (2014), Weakening of the stratospheric polar vortex by Arctic sea-ice loss, *Nature Communications, 5,* 4646.

King, M. P., M. Hell, and N. Keenlyside (2015), Investigation of the atmospheric mechanisms related to the autumn sea ice and winter circulation link in the Northern Hemisphere, *Clim. Dyn.,* doi:10.1007/s00382-015-2639-5.

Kug, J. S., J. H. Jeong, Y. S. Jang, B. M. Kim, C. K. Folland, S. K. Min, and S. W. Son (2015), Two distinct influence of Arctic warming on cold winters over North America and East Asia, *Nature Geoscience, 8,* 759–762.

Liu, J. P., J. A. Curry, H. Wang, M. Song, and R. M. Horton (2012), Impact of declining Arctic sea ice on winter snowfall, *Proc. Natl. Acad. Sci., 109,* 4074–4079.

Manzini, E., M. A. Giorgetta, M. Esch, L. Kornblueh, and E. Roeckner (2006), The Influence of Sea Surface Temperatures on the Northern Winter Stratosphere: Ensemble Simulations with the MAECHAM5 Model, *J. Clim., 19,* 3863–3881.

382 Mori, M., M. Watanabe, H. Shiogama, J. Inoue, and M. Kimoto (2014), Robust Arctic
383 sea-ice influence on the frequent Eurasian cold winters in past decades, *Nature*
384 *Geoscience, 7,* 869–873.
385 Nakamura, T., K. Yamazaki, K. Iwamoto, M. Honda, Y. Miyoshi, Y. Ogawa, and J.
386 Ukita (2015), A negative phase shift of the winter AO/NAO due to the recent Arctic
387 sea-ice reduction in late autumn, *J. Geophys. Res., 120,* 3209–3227.
388 Nishii, K., H. Nakamura, and Y. J. Orsolini (2011), Geographical dependence observed
389 in blocking high influence on the stratospheric variability through enhancement or
390 suppression of upward planetary-wave propagation, *J. Clim., 24,* 6408–6423.
391 Orsolini, Y. J., R. Senan, R. E. Benestad, A. Melsom (2012), Autumn atmospheric
392 response to the 2007 low Arctic sea ice extent in coupled ocean-atmosphere hindcasts,
393 *Clim. Dyn., 38,* 2437–2448. doi:10.1007/s00382-011-1169-z
394 Overland, J., K. Wood, and M. Wang (2011), Warm Arctic - cold continents: climate
395 impacts of the newly open Arctic Sea, *Polar Research, 30,* 15787.
396 Peings, Y., D. Saint-Martin, and H. Douville (2012), A Numerical Sensitivity Study of
397 the Influence of Siberian Snow on the Northern Annular Mode, *J. Clim., 25,* 592–607.
398 Plumb, R. A. (1985), On the Three-Dimensional Propagation of Stationary Waves, *J.*
399 *Clim., 42,* 217–229.
400 Screen, J. A., and I. Simmonds (2014), Amplified mid-latitude planetary waves favour
401 particular regional weather extremes, *Nature Climate Change, 4,* 704–709.
402 Smith, K. L., C. G. Fletcher, and P. J. Kushner (2010), The role of linear interference in
403 the Annular Mode response to extratropical surface forcing, *J. Clim., 23,* 6036–6050.
404 Sun, L., C. Deser, and R. A. Tomas (2015), Mechanisms of stratospheric and
405 tropospheric circulation response to projected Arctic sea ice loss, *J. Clim., 28,* 7824–
406 7845.
407 Thompson, D. W. J., and J. M. Wallace (1998), The Arctic Oscillation signature in the
408 wintertime geopotential height and temperature fields, *Geophys. Res. Lett., 25,* 1297–
409 1300.
410 Thompson, D. W. J., and J. M. Wallace (2001), Regional Climate Impacts of the
411 Northern Hemisphere Annular Mode, *Science, 293,* 85–89.
412 Vavrus, S., J. E. Walsh, W. L. Chapman, and D. Protis (2006), The behavior of extreme
413 cold air outbreaks under greenhouse warming, *Int. J. Climatol., 26,* 1133–1147,
414 doi:10.1002/joc.1301.

Wegmann, M., Y. Orsolini, M. Vázquez, L. Gimeno, R. Nieto, O. Bulygina, R. Jaiser, D. Handorf, A. Rinke, and K. Dethloff (2015), Arctic moisture source for Eurasian snow cover variations in autumn, *Environ. Res. Lett., 10,* 054015.

Table 1. Outline of experiments. *Early* (1979–1983) and *Late* (2005–2009) are the time periods for which monthly average sea surface temperature (SST) or sea-ice thickness (SIT) was used for the boundary conditions.

Experiment	Run	Integration period (years)	Zonal mean zonal wind restoration	SST	SIT
FREE	*HICE*	60	N/A	*Early*	*Early*
	LICE				*Late*
RS10	*HICE*	60	Above 10 hPa	*Early*	*Early*
	LICE				*Late*
RS30	*HICE*	60	Above 30 hPa	*Early*	*Early*
	LICE				*Late*

Figure captions

Figure 1. December-January-February averaged anomalies (*LICE* minus *HICE*) of **a,** geopotential height at 50 hPa (in m); **b,** geopotential height at 300 hPa (m); and **c,** temperature at 2 m height (K) in the (from left to right) *Free*, *RS10* and *RS30* experiments. *LICE* and *HICE* runs indicate perpetual model simulations with annual cycle of low (2005–2009) and high (1979–1983) sea-ice conditions, respectively (see Methods). In **a** and **b**, red (blue) contours indicate amplitudes of the positive (negative) anomaly, with the zero line omitted. Light and heavy grey shades indicate statistical significance greater than 95% and 99%, respectively. In **c**, red (blue) shading indicates positive (negative) anomalies. Hatching (cross-hatching) indicates statistical significance greater than 95% (99%).

Figure 2. a, Time–height cross sections of daily mean anomalies (*LICE* minus *HICE*) of zonal mean zonal wind at 60°N. Red (blue) contours indicate amplitudes of the positive (negative) anomaly, with the zero line omitted. Light and heavy grey shades indicate statistical significance greater than 95% and 99%, respectively; the contour interval is 2.0 m s^{-1}. **b,** Time series of daily anomalies of Fz (vertical component of the

441 Eliassen-Palm flux) at 100 hPa averaged over 50–80°N. Black dot indicates the
442 statistical significance greater than 95%. Purple line segments signify periods when the
443 Fz anomaly exceeded 10^4 m^2 s^{-2}. **c,** Lead-lag correlation coefficients of polar cap height
444 (PCH) at various pressure levels with PCH at 100 hPa. Red (blue) shading indicates
445 positive (negative) correlations; contour interval is 0.1.
446
447 **Figure 3.** January *LICE*-minus-*HICE* anomalies of **a,** geopotential height at 100 hPa
448 (m) and **b,** vertical component of the wave activity flux at 100 hPa (10^3 m^2 s^{-2}).
449 Contours indicate amplitudes of the anomaly with the zero line omitted. Light and
450 heavy grey shadings indicate statistical significance over 95% and 99%, respectively.
451

Figures

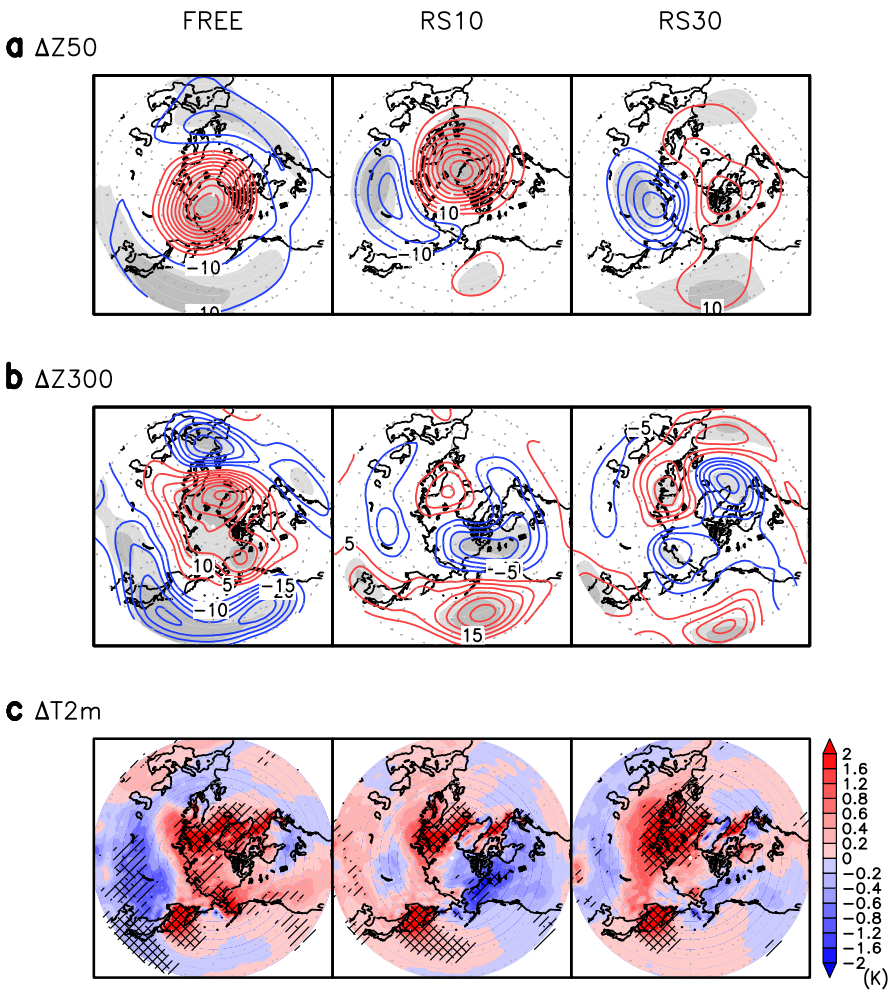

Figure 1. December-January-February averaged anomalies (*LICE* minus *HICE*) of **a,** geopotential height at 50 hPa (in m); **b,** geopotential height at 300 hPa (m); and **c,** temperature at 2 m height (K) in the (from left to right) *Free*, *RS10* and *RS30* experiments. *LICE* and *HICE* runs indicate perpetual model simulations with annual cycle of low (2005–2009) and high (1979–1983) sea-ice conditions, respectively (see Methods). In **a** and **b**, red (blue) contours indicate amplitudes of the positive (negative) anomaly, with the zero line omitted. Light and heavy grey shades indicate statistical significance greater than 95% and 99%, respectively. In **c**, red (blue) shading indicates positive (negative) anomalies. Hatching (cross-hatching) indicates statistical significance greater than 95% (99%).

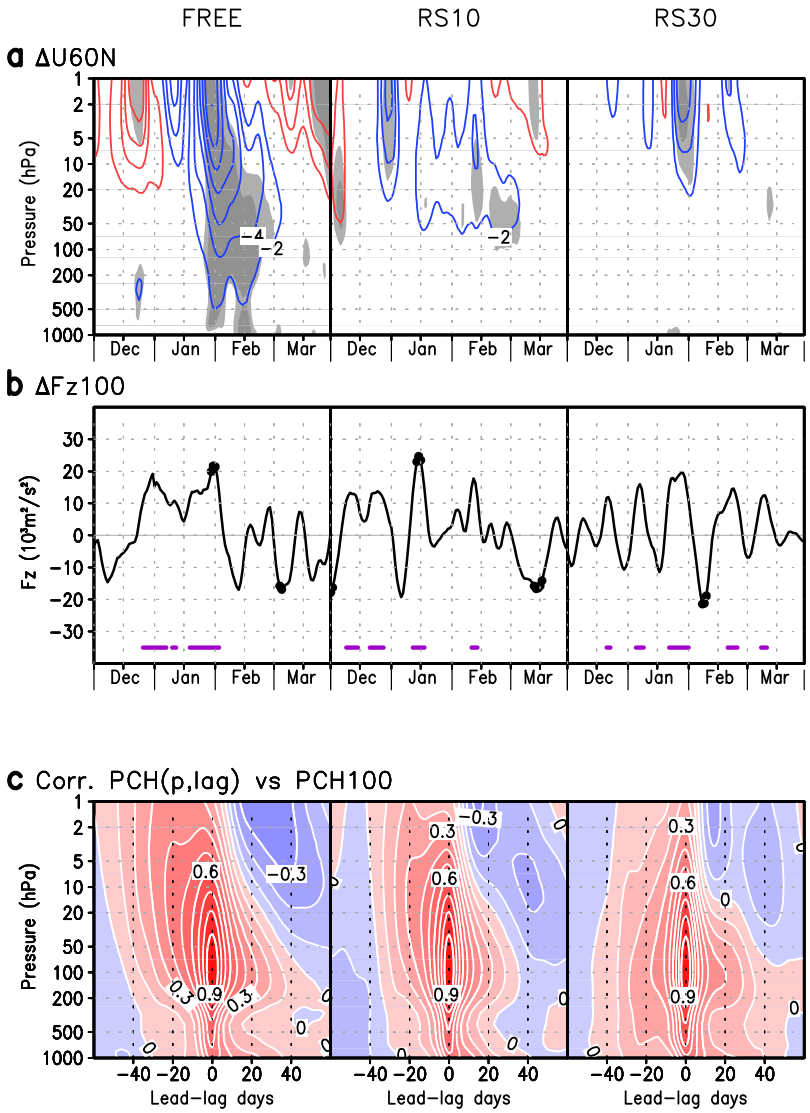

Figure 2. a, Time–height cross sections of daily mean anomalies (*LICE* minus *HICE*) of zonal mean zonal wind at 60°N. Red (blue) contours indicate amplitudes of the positive (negative) anomaly, with the zero line omitted. Light and heavy grey shades indicate statistical significance greater than 95% and 99%, respectively; the contour interval is 2.0 m s^{-1}. **b,** Time series of daily anomalies of Fz (vertical component of the Eliassen-Palm flux) at 100 hPa averaged over 50–80°N. Black dot indicates the statistical significance greater than 95%. Purple line segments signify periods when the Fz anomaly exceeded 10^4 m^2 s^{-2}. **c,** Lead-lag correlation coefficients of polar cap height (PCH) at various pressure levels with PCH at 100 hPa. Red (blue) shading indicates positive (negative) correlations; contour interval is 0.1.

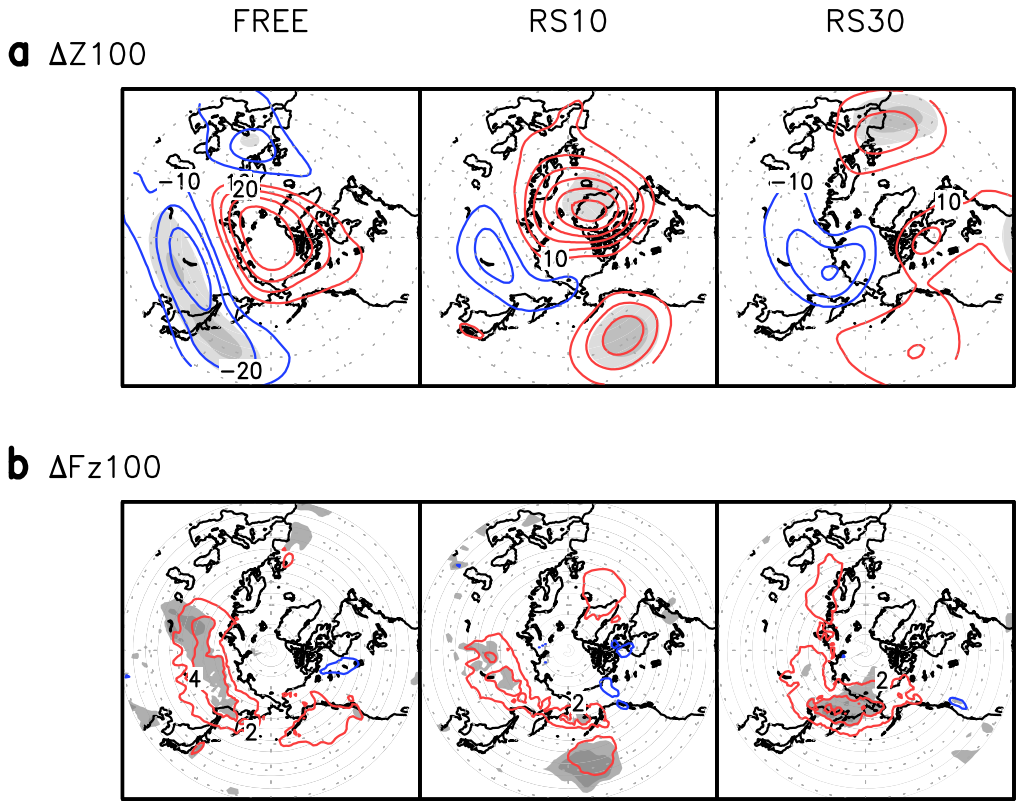

476

477 **Figure 3.** January *LICE*-minus-*HICE* anomalies of **a,** geopotential height at 100 hPa
478 (m) and **b,** vertical component of the wave activity flux at 100 hPa (10^3 m^2 s^{-2}).
479 Contours indicate amplitudes of the anomaly with the zero line omitted. Light and
480 heavy grey shadings indicate statistical significance over 95% and 99%, respectively.

481

482

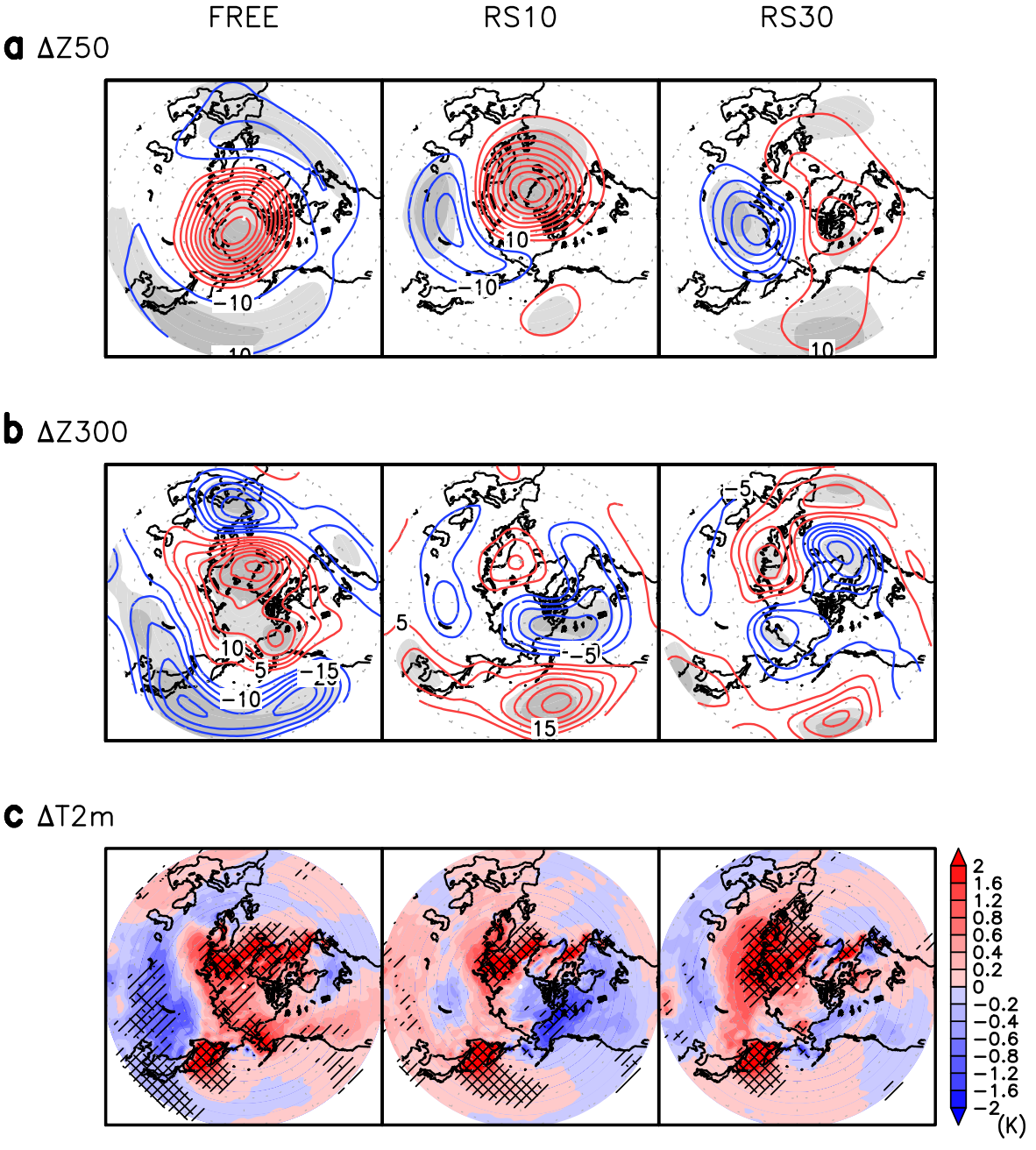
FREE
RS10
RS30
a ΔZ50
−10
10
10
10
−10
10
b ΔZ300
10
5
−15
−10
5
−5
15
−5
c ΔT2m
2
1.6
1.2
0.8
0.6
0.4
0.2
0
−0.2
−0.4
−0.6
−0.8
−1.2
−1.6
−2
(K)

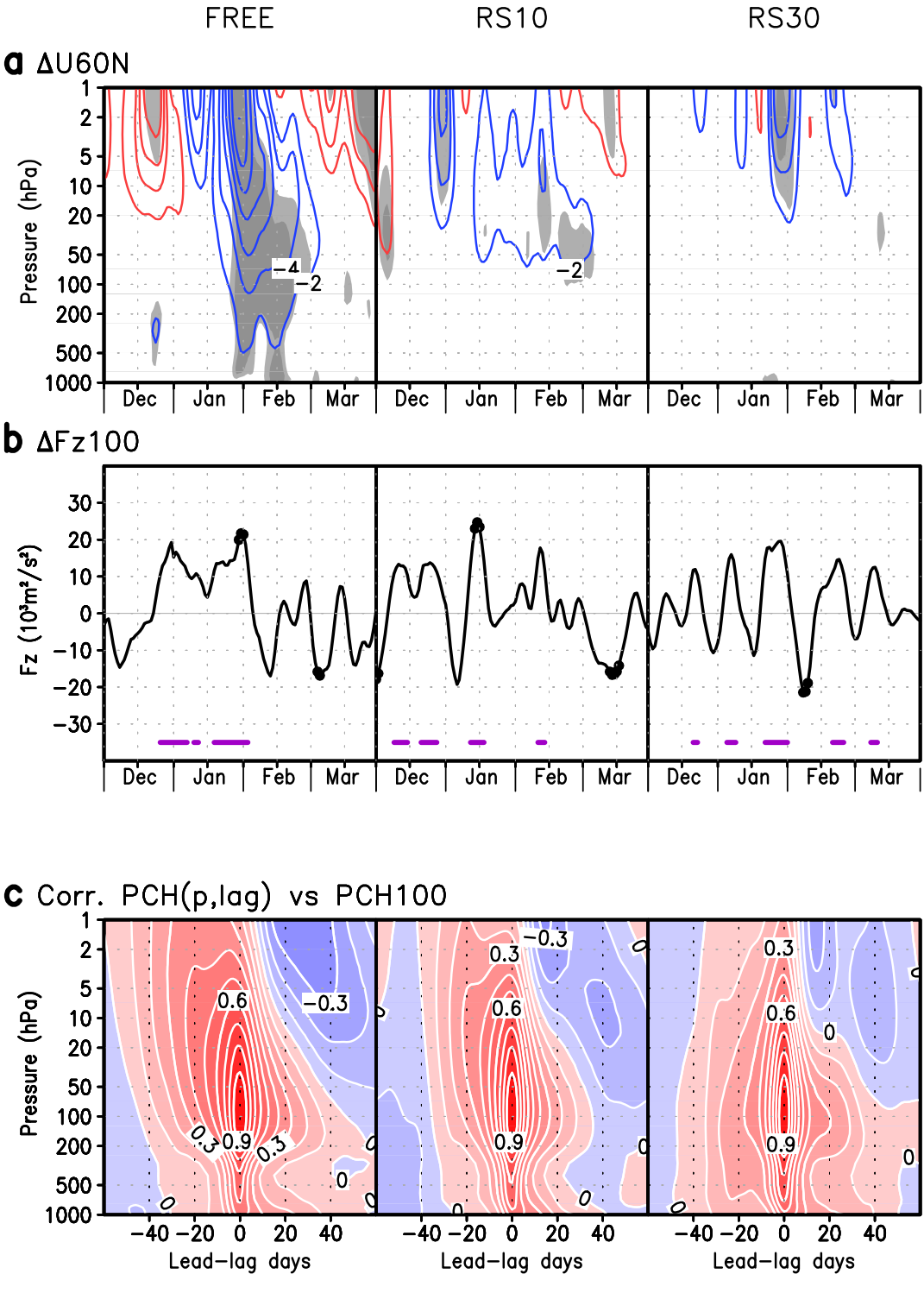
FREE
RS10
RS30
a ΔU60N
Pressure (hPa)
1
2
5
10
20
50
100
200
500
1000
−4
−2
−2
Dec
Jan
Feb
Mar
b ΔFz100
Fz (10³m²/s²)
30
20
10
0
−10
−20
−30
c Corr. PCH(p,lag) vs PCH100
0.6
−0.3
0.3
0.9
0
Lead−lag days
−40
−20
0
20
40

FREE RS10 RS30

a ΔZ100

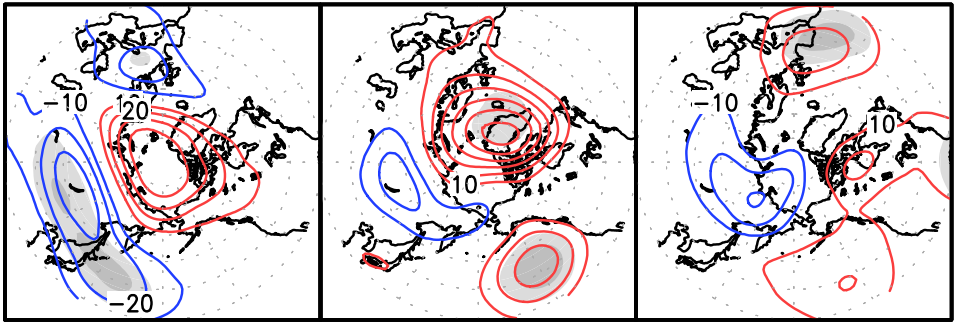

b ΔFz100